Application of principal-components based invariant display strategy to wide-area hyperspectral data

J. Scott Tyo[a], Athanasios Konsolakis[a], David I. Dierson[a], and Richard C. Olsen[b]

[a]Electrical and Computer Engineering Department
[b]Physics Department
Naval Postgraduate School
Monterey, CA 93943

ABSTRACT

A principal components (PC)-based transformation was previously introduced for mapping high-dimensional hyperspectral imagery (HSI) into 3-dimensional colorimetric displays [Tyo, Diersen, and Olsen, *SPIE vol. 4132*, Descour and Shen, Eds., 2001, pp. 147–156]. In this study, the previous work is extended to examine the conical nature of HSI data in the PC-based space. Picturing the data as conical provides insight as to the location of the origin of the cone (which might not be included in the data) and the point of shade. Once the origin of the cone is located, the PC-based color transformation is more stable with respect to hue constancy. Strategies are introduced to make the method invariant, i.e. to ensure that important scene constituents appear with consistent and intuitive presentations.

Keywords: Spectral Imagery, Display Strategies, Colorimetric Representations

1. INTRODUCTION

Hyperspectral imagery (HSI) has emerged as a potentially powerful tool for locating and identifying objects and materials in remotely sensed imagery. While numerous tools have been developed to classify materials and locate objects in HSI scenes, the most common strategies for displaying the information involve mapping some subset of the HSI data into a grayscale or RGB image, with the possible addition of cues to the image to direct attention to particular areas of interest.

HSI data is vastly different from conventional visible spectrum imagery. First, HSI sensors have hundreds of spectrally narrow and contiguous spectral bands, providing high spectral resolution data about the material makeup of objects within a scene.[1] Second, the sensors often extend to regions of the spectrum where the human vision system is not sensitive, namely the near, short-,[2,3] mid-, and long-wave infrared[4] and ultraviolet[5] spectral regions. There is a long history of interpreting infrared imagery, but in the past the sensors have been panchromatic and intensity could be related to temperature and emmissivity. With HSI data, there is spectral structure in these regions, and a new approach must be developed to present that variation in the final imagery.

The two most common approaches to mapping HSI data into pseudocolor involve mapping band data or principal components data at each pixel into a RGB triple. In the former strategy, the user would select three HSI bands in the hopes of capturing either large-scale image variations or particular spectral features. An example of such a mapping is presenting a long-, mid-, and shortwavelength visible band as and RGB image. This approximates what a human observer would see if they were actually looking at the scene. An example of this mapping strategy are shown in fig. 1. This class of mapping strategy can be very powerful, as highly specialized colormaps can be designed that are tailored to particular applications, such as locating a specific spectral feature throughout a scene. However, there are some drawbacks associated with this strategy. First, any spectral feature that does not overlap with chosen bands will not be represented. Second, there is no a-priori way to predict the color representation in the final images or interpret them.

A second strategy attempts to solve some of those drawbacks. It involves taking a principal components (PC) transformation and mapping the resulting PC images into an RGB triple. Examples of such images are presented in fig. 2. The PC images are formed by diagonalizing the covariance matrix of the data, and projecting the HSI scene onto the resulting (orthogonal) eigenvectors. The eigenvectors are linear combination variables that include

Authors' email addresses: tyo@ieee.org, olsen@nps.navy.mil
J. S. Tyo is currently with the EECE Dept., University of New Mexico, Albuquerque, 87131

Imaging Spectrometry VII, Michael R. Descour, Sylvia S. Shen, Editors,
Proceedings of SPIE Vol. 4480 (2002) © 2002 SPIE · 0277-786X/02/$15.00

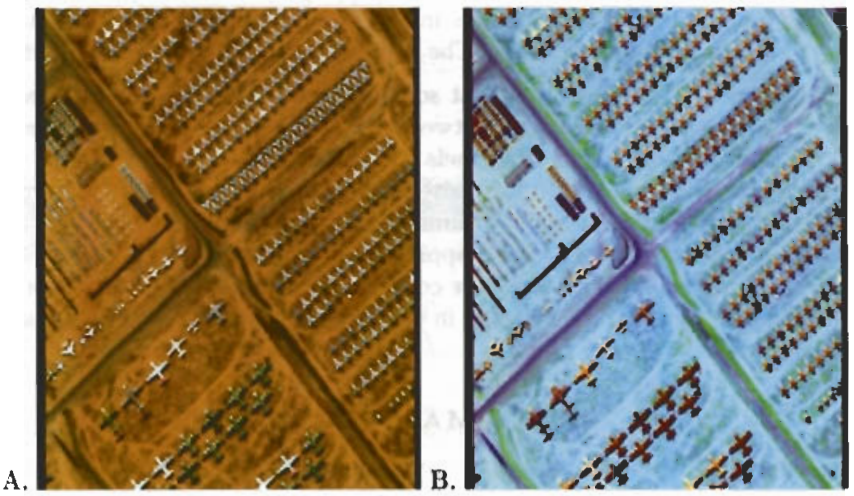

Figure 1. Two common three-color mapping strategies. The data is HYDICE data from Davis Monthan AFB. The first image maps bands at 630 nm, 550 nm, and 450 nm into R, G, and B. This is an approximation of what a human observer would see. The second image presents bands at 600nm, 1000 nm, and 2000 nm, and shows widely spaced spectral bands.

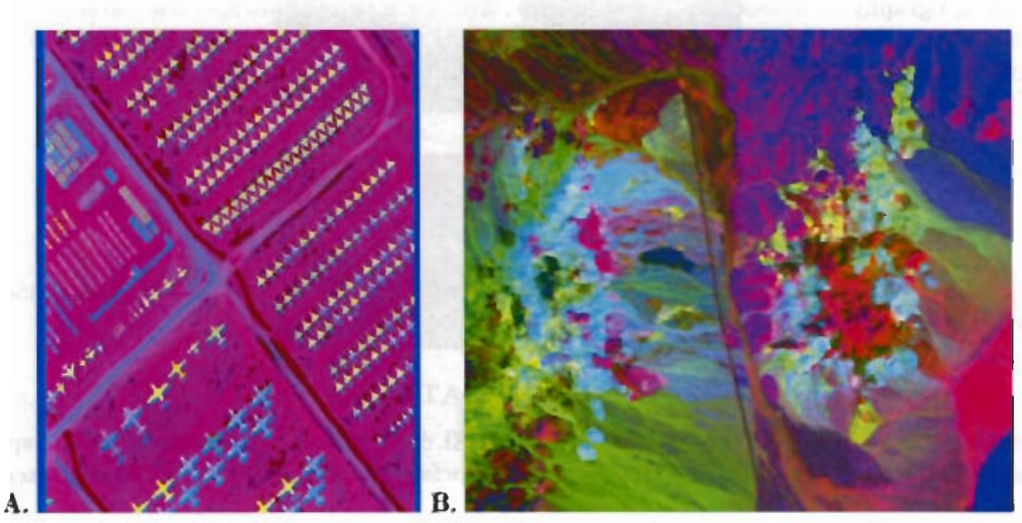

Figure 2. Mapping PC images into RGB triples. A. The HYDICE DM data with the 1st PC mapped into red, 2nd PC into green, and 3rd PC into blue. B. SWIR (1.9 - 2.5 μm AVIRIS) data from Cuprite, NV.

the spectral features that contribute most to the scene variance. They represent statistically uncorrelated channels and are ordered in decreasing amounts of scene variance. The derived variable sample information from across the scene, and reduce the chances that an important spectral feature (from a variance standpoing) will be missed in the final representation. The problem with the mappings in fig. 2 is that they map orthogonal data (PC images) into non-orthogonal display channels (RGB intensities). The result is an image that is often difficult to interpret.

Recently, a PC-based strategy was presented that sought to eliminate the problems associated with the above mapping.[6] That strategy exploits the similarities between HSI data and human color vision. The orthogonal PC channels are mapped into orthogonal display channels in an ergonomic manner. The end goal is to derive an invariant mapping strategy for HSI data that consistently and intuitively represents important scene constituents in the final scene. Advanced processing methods can simultaneously be applied to the HSI data, enabling overlay of identification information. In section section 2 the mapping strategy is reviewd. In section 3 the data is examined in the transformed space and analyzed for suitability for colorimetric mapping. Section 4 contains descriptions of two new tools being investigated for use with the strategy in order to achieve invariance. Discussions and conclusions are in section 4 and 5 respectively.

2. PC-BASED MAPPING STRATEGY

The close relationship between HSI data and human color vision was discussed previously.[6] A PC analysis of the human photoreceptor spectral response produces three statistically orthogonal channels – one that is roughly achromatic, one that is a difference between long- and mid- wavelength spectral content (red - green), and a third that is trimodal, and nominally represents the difference between short- and mid- wavelength information (blue - yellow).[7] These three orthogonal dimensions can be used to define orthogonal directions in a 3-dimensional, conical data space.[8] The three coordinates hue (angle within the R-G/B-Y plane), saturation (radius in the R-G/B-Y plane divided by total intensity), and value (total intensity) give location within the cone and are commonly used for constructing pseudocolor images.

Analysis of HSI data yields a 1st PC that is usually related to the average scene illumination. That channel typically has slow spectral variation (except in atmospheric absorption bands) and closely resembles the solar distribution convolved with the atmospheric transmission. When an image is dominated by a particular material, that spectral signature might also contribute significantly to the scene variance and may show up in the 1st PC as well. The 1st PC image contains a basic panchromatic intensity image and has much of the high spatial frequency information often associated with geography. Successiveley higher PCs tend to have more rapid spectral variations. The higher PCs also have lower-spatial frequency information that is typically associated with regions of like spectral content. The close analogy between the HSI and color vision analyses leads to the proposed mapping strategy

$$\begin{array}{rcl} \phi = \text{atan}\left(\frac{P_3}{P_2}\right) & \rightarrow & H \\ \rho = \frac{\sqrt{{P_2}^2+{P_3}^2}}{P_1} & \rightarrow & S \\ P_1 & \rightarrow & V \end{array} , \tag{1}$$

where P_1, P_2, and P_3 are the 1st , 2nd , and 3rd PC values and H, S, and V are the hue, saturation and value. The basic properties of this transformation have been discussed previously.[6]

3. CONICAL DATA SPACE

The transformation in (1) projects the high-dimensional HSI data into a 3-dimensional conical space. That space is tightly bunched about the P_1 axis, since the variance associated with the 1st PC is often in excess of 90% of the total scene variance.[6]

To illustrate the effects of this transformation on HSI data, the 50-band AVIRIS data of Cuprite, NV, that is distributed with the ENVI software package has been analyzed. This data covers portions of the SWIR spectrum from 1.9 - 2.5 μm. A scatterplot of the data in 3-dimensional space is presented in fig. 3. The data in fig. 3 represent $\frac{1}{12}$ of the total pixels so that the major trends can be seen. An implementation of (1) for this data is presented in fig. 4.

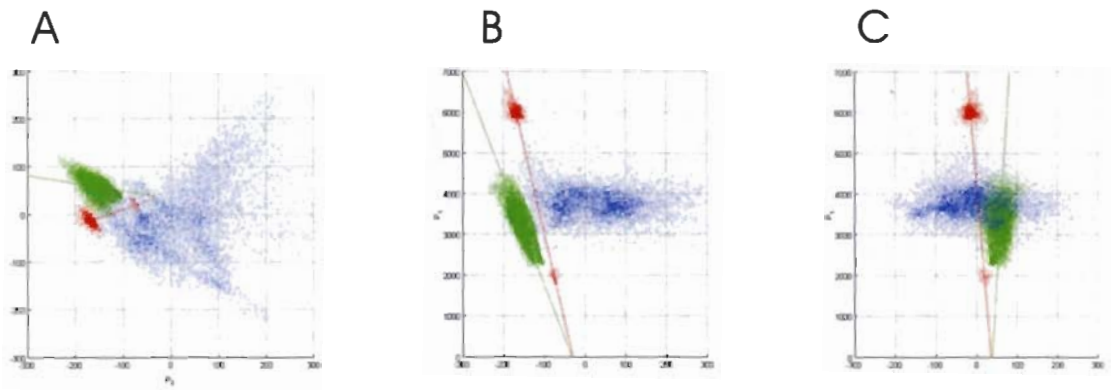

Figure 3. Scatterplots. A. Cone projected onto the $P_2 - P_3$ plane, B. $P_2 - P_1$ plane. C. $P_3 - P_1$ plane. The numerical values presented here represent absolute projections of the HSI data at each pixel onto the eigenvectors of the covariance matrix of the data with no scaling or translation.

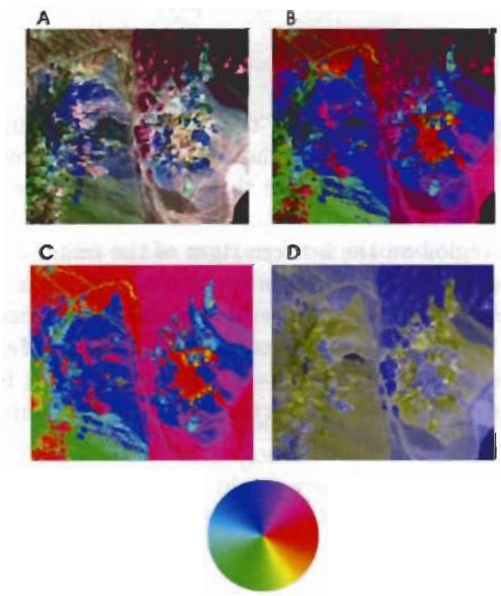

Figure 4. Four representations of the AVIRIS Cuprite data using (1). A. Full implementation with saturation stretched to maximum dynamic range. B. Suppression of saturation information by setting $S = 1$ everywhere. C. Hue only, setting $S = 1$ and $V = 1$ everywhere. D. Projection of (1) into the $B - Y$ plane.

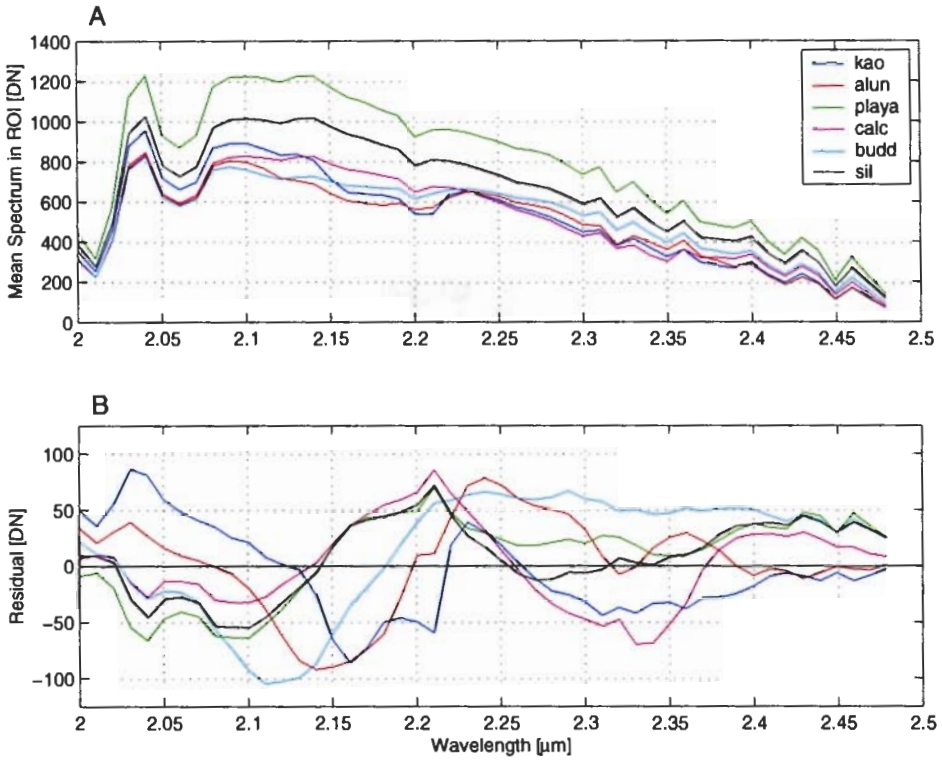

Figure 5. Five different material mean spectra obtained by averaging over a ground-truthed region of the data. A. Mean spectrum. B. Residual remaining after subtracting the projection of the mean spectrum onto the 1st PC

3.1. Location of the Origin

The conical nature of the data in fig. 3 is highlighted by the lines drawn through two major groups within the data. The green data represents a collection of pixels from the mountainous region in the top right of the image. The views from the *side* of the cone (fig. 3B and C) indicate that these points are radiating out from a common origin. The two groups of red pixels in fig. 3 represent high- and low-intensity pixels with similar spectral features. The brighter of the two is from the playa region on the bottom right of the image and the darker is from the dark spot in the center of the image. These two groups seem to lie in a common direction within the cone in panels B and C of fig. 3, and a linear fit to these data is drawn in the scatterplot in red. Even though the lowest intensity (P_1) value in the image is at a digital number of 1732, the two lines extrapolate back until they almost intersect near the $P_1 = 0$ plane. However, this point of intersection is not at $P_2 = 0$, $P_3 = 0$, rather it is offset somewhat and represents the "point of shade," or the vertex of the cone. Once the vertex of the cone is found, the values of ϕ and ρ in (1) should be referenced to that vertex. The image presented in fig. 4 has been reoriented accordingly.

The method of finding the vertex described above might be termed semi-autonomous. The manual part of the process involves identifying pixels with like spectral characteristics that can be assumed to lie in the same direction within the cone. Once those pixels have been identified, the least squares regressions can be computed automatically to locate the origin. This process is laborious and somewhat subjective. A means of finding the origin completely automatically is the subject of future research.

3.2. Material classification

The procedures outlined in this study are not a classification method *per se*; however, the manner in which various materials are presented is of interest. A number of pixels have been identified from gound-truth observations as containing specific materials.[NEED THE REF] A set of seven regions of interest (ROIs) is distributed with ENVI. The mean spectrum in each of these regions is presented in fig. 5. To find the region of the scatterplot of fig. 3

Material	$L \cdot P_1$	$L \cdot P_2$	$L \cdot P_3$	Angle	Saturation	Color
Calcite	4010	-96	-76.6	$-143°$	0.030	
Alunite	3810	169	217	52.8°	0.073	
Kaolinite	4060	294	-34.1	$-5.46°$	0.073	
Buddingtonite	3980	-79.0	301	104°	0.080	
Silica	4990	-217	29.2	170°	0.032	
Playa	6020	-196	69.0	159°	0.035	
Varnished Tuff	3590	-176	92.2	151°	0.056	

Table 1. Projection of the mean material spectra on the first three PCs, as well as angle in the $P_2 - P_3$ plane as indicated in the scatterplot of fig. 3.

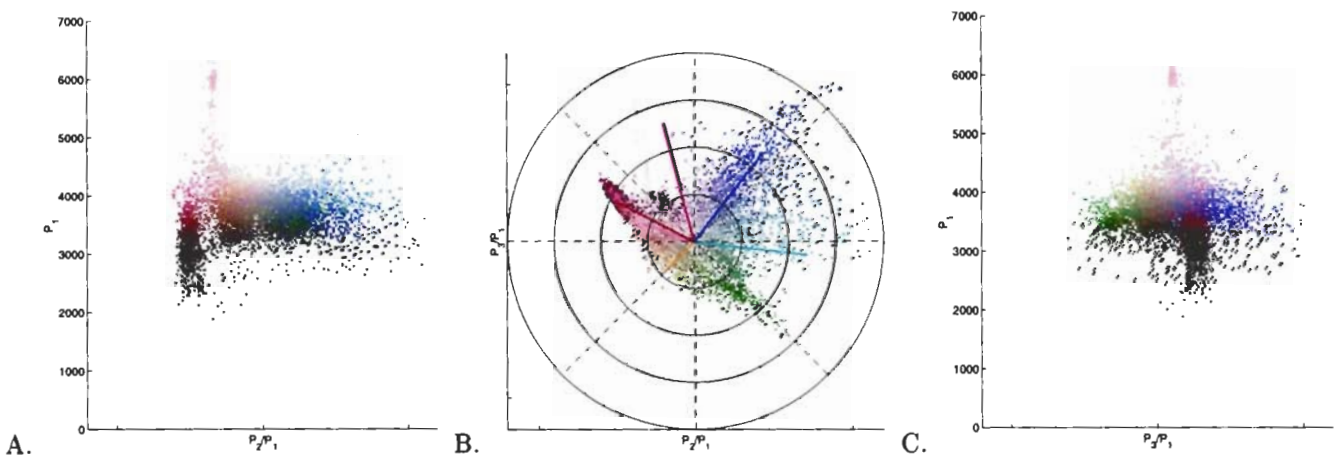

Figure 6. The scatterplot of fig. 3 with the x- and y-coordinate normalized to the z-coordinate. The effect is to turn the cone if fig. 3 into a cylinder. Each point in the scatterplot is colored the same as in the mapping of fig. 4A. The data set has been thinned by a factor of 20 to aid in viewing. Unsaturated (gray) pixels are those near the origin, and particular hues radiate outwards. A. $P_2 - P_1$ plane. B. $P_3 - P_1$ plane. C. $P_2 - P_3$ plane. The lines represent the average material spectra from table 1.

corresponding to each of these mean spectra, a projection is taken on the first three PCs. The residual spectra is defined here as the portion of the radiance vector orthogonal to the P_1 axis. It is computed by

$$\underline{\mathbf{x}}_{resid} = \underline{\mathbf{x}} - \left(\underline{\mathbf{x}}^{\mathrm{T}} \underline{\mathbf{v}}_1\right) \cdot \underline{\mathbf{v}}_1. \tag{2}$$

Classification information is held in the residual spectra. For each of the materials, an angle in the $P_2 - P_3$ plane was computed by taking the appropriate projections (referenced to the origin found above), and the results are summarized in table 1.

The scatterplot of the data is shown again in fig. 6 projected onto the $P_2 - P_3$ plane. Each point in the scatterplot is colored with the same (H, S, V) values as the corresponding pixel in fig. 4A. Lines radiation from the origin to the location of the ROI means in table 1 are also superimposed on the data.

4. DISCUSSION

The strategy outlined above has several advantages and disadvantages that are worth mentioning. First, the mapping capitalizes on similarities between the PC channels in HSI and color vision to create an ergonomic strategy that preserves orthogonality relationships in the final mapping. The spatial frequency structure of the PC images in HSI nicely match the spatial sensitivity of the corresponding color channels. This match points towards a possible compression strategy, namely a hybrid spatial/spectral compression scheme that uses information about the spatial frequency structure of higher PC channels to reduce noisy and/or less important data from a scene. This is the strategy that has been utilized by human vision. High spatial frequency information that is presented in the $(R - G)$ and $(B - Y)$ channels is not readily perceived,[9] helping to minimize the bandwidth necessary to process color scenes.[7]

Fig. 6 and table 1 demonstrate the classification features of the PC based strategy defined above. Materials with significant spectral differences will map into hues that are well-separated, and materials with similar spectral features map into similar hues. This feature can also be a negative, though, as closely related materials that can be reliable differentiated using some processing strategy may not be as distinguishable using the mapping described above. However, the mapping discussed here is not a classifier in that it does not make a decision about the presence or absence of any particular material in a pixel.

One of the features of fig. 1 and fig. 4A that makes them more accessible to human observers is that much of the image is largely desaturated (gray). In contrast, the images in fig. 2 are highly saturated everywhere, giving rise to apparent smearing between colors. Regions of the image that do not have any significant spectral deviation from the average illumination have little or no projection onto the 2^{nd} and 3^{rd} PCs that determine the color in (1). Hence, they are not represented with pure hues. The mapping presented in fig. 4B suppresses saturation, allowing determiniation of the hue that most closely matches each pixel. In that way, the parameter saturation is equivalent to a confidence measure in the same sense that the parameter hue is equivalent to a material classification.

There is a fundamental problem associated with the mapping of high-dimensional HSI data into a pseudocolor image. Because of the 3-dimensional nature of color vision, any strategy must be lossy in that the full dimensionality of the HSI data cannot be represented. Furthermore, typical HSI sensors collect data from outside the visible spectrum. This means that at least some information must be presented that the human observer is not used to interpreting. A good example of this is highlighted with the Cuprite data analyzed above. The entire data set is from the SWIR (1.9 - 2.4 μm). In the visible portion of the spectrum, this is a very uninteresting scene and appears almost uniformly as a dull brownish color. The mappings presented in fig. 4 force color where none existed before, and this strategy will necessitate some training of observers for maximum benefit.

4.1. Invariant Display Strategies

The long-term goal of this project is the development of an invariant display strategy that can be broadly applied to HSI data. The direct implementation of (1) is not an invariant strategy, since the PCs are calculated from *in scene* statistics. Furthermore, implementation of (1) does not guarantee that materials are going to be presented in hues that are intuitive to the observer. For example, what happens if water just happens to map into a hue associated with the color red? Below we discuss two new techniques that are being investigated to hande these problems.

4.1.1. In-Scene vs. Non-In-Scene Eigenvectors

The derived eigenvectors are different for every scene, therefore a single spectrum would have different representations from image to image. Analysis of several contiguous scenes from Davis Monthan AFB demonstrated that the first three eigenvectors had significant variations even in scenes where there is a large amount of spectral correlation.[10] When comparing two dissimilar scenes, the differences can be quite severe. Ideally, a set of orthogonal eigenvectors could be developed that capture a large part of the spectral information for a variety of applications. These eigenvectors could be used to create a standard mapping similar to the tasseled cap transformation that is commonly applied with multispectral LANDSAT imagery.[11]

As an example, consider the scene presented in fig. 7. The scene is a full AVIRIS image cube of a shore region of Lake Tahoe, CA. It is a relatively simple scene with water in the upper left, forest in the lower right, and a shoreline transition region. Fig. 8 shows the eigenvectors from the scene covariance matrix. There are important features of the target spectra that deviate markedly from the mean solar spectrum. Because the scene is dominated by two

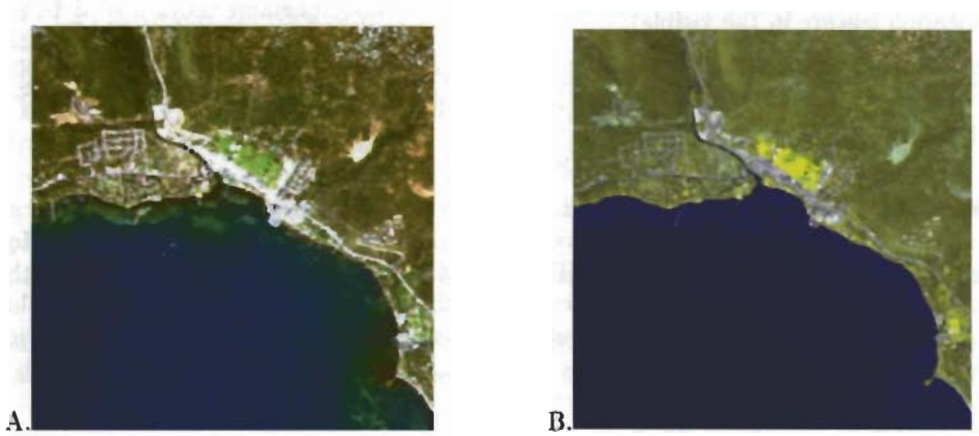

Figure 7. Images of Lake Tahoe, CA. A. RGB image using bands at $\lambda = 639\,\text{nm}$, $\lambda = 549\,\text{nm}$, $\lambda = 429\,\text{nm}$. B. Post-rotated version using (1). Hues were rotated after transformation to ensure that the water was "blue" and the forest was "green". The only post processing that occurred was a rotation of the hue by 75°.

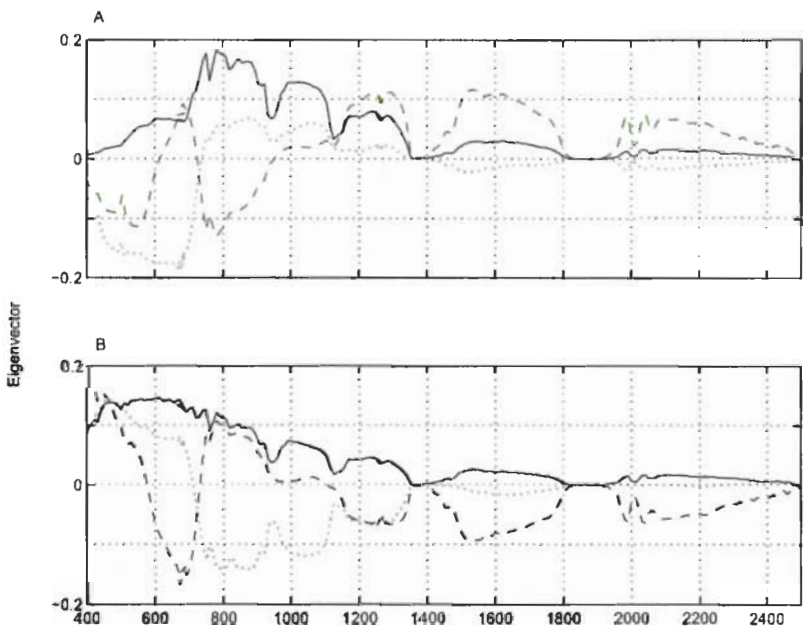

Figure 8. First three eigenvectors from Tahoe scene. A. Eigenvectors computed from in-scene statistics. B. First eigenvector determined externally (extracted from Davis Monthan AFB average radiance). In panel B, the 2nd and 3rd eigenvectors were determined from in-scene statistics. Note that in panel A, the first eigenvector is largely influenced by the chlorophyll absortption feature in the NIR. Also note that in the SWIR, the 2nd eigenvector in panel B has much less weight.

primary constituents, the 1st eigenvector has spectral features of the targets as well as the illumination (namely the chlorophyll absorption feature in the visible).

As a step in developing an invariant strategy, a standard 1st eigenvector that is computed from known solar and atmospheric properties was forced on the data. This was accomplished by means of a Gramm-Schmid orthogonalization whereby the covariance matrix of

$$\underline{\mathbf{y}} = \underline{\mathbf{x}} - (\underline{\mathbf{x}} \cdot \hat{\underline{\mathbf{v}}})\hat{\underline{\mathbf{v}}} \tag{3}$$

was orthogonalized. In (3) $\underline{\mathbf{x}}$ is the data vector and $\hat{\underline{\mathbf{v}}}$ is a unit vector corresponding to a reference spectrum obtained by some other method (in this case the first eigenvector was taken from an HSI image of Davis-Monthan AFB). The new reference eigenvectors are depicted in fig. 8C. The target information has been removed from the first eigenvector and now all target information appears in the second and third channels. *. Similar steps could be performed to create the 2nd and 3rd eigenvectors, and the resulting transformation could have a colorimetric mapping that is stable, intuitive, and ergonomic.

4.1.2. Post-Rotation of the RGB Data

Sometimes it may be desired to use the in-scene statistics to compute the eigenvectors for transformation. These eigenvectors give the best ordering of the in-scene variance, and highlight the most important features of the particular image. However, use of in-scene statistics will lead to colormaps that are not always intuitive. A method for overcoming this difficulty is proposed in this section.

When the spectral data includes bands in the visible, a 3-color composite image can be constructed that closely mimics what a human observer would see. In fig. 7, an important scene constituent is the water. The color transformation can be rotated to ensure that the materials that closely resemble water are presented with a particular hue, i.e. the color blue. The mapping presented in fig. 7B was computed using such a post-rotation. The 2nd and 3rd eigenvectors were still obtained using in-scene data. If a strategy is developed to arrive at global eigenvectors, then (1) can be appropriately modified to ensure that important materials are presented in a standard form. We are also exploring a strategy that using the data from the visible spectrum to automatically implement this rotation, as introduced by Diersen.[10]

5. CONCLUSIONS

A colorimetric display strategy based on principal componenets analysis and mapping previously introduced has been discussed.[6] The conical data space that is implied in this mapping has provided information about the structure of the data. A supervised method for locating the origin of this cone has been developed, and might be important for locating the point of shade in HSI data. The mapping was shown to differentiate between certain types of materials, and represent the result in an ergonomic fashion.

There remains significant work to develop an invariant display strategy based on PC analysis. All methods implemented thus far rely in some fashion on in-scene statistics, which by-definition are not invariant. Strategies were discussed above to overcome this limitation, and are currently under investigation.

REFERENCES

1. A. F. H. Goetz, "Imaging spectrometry for remote sensing: Vision to reality in 15 years," in *Proceedings of SPIE vol. 2480, Imaging Spectrometry*, M. R. Descour, M. J. Mooney, D. L. Perry, and L. Illing, eds., pp. 2–13, SPIE, (Bellingham, WA), 1995.
2. G. Vane, R. Green, T. Chrien, H. Enmark, E. Hansen, and W. Porter, "The airborne visible infrared imaging spectrometer," *Remote Sensing Environ.* **44**, pp. 127–143, 1993.
3. R. W. Basedow, D. C. Armer, and M. E. Anderson, "Hydice system: Implementation and performance," in *Proceedings of SPIE vol. 2480, Imaging Spectrometry*, M. R. Descour, M. J. Mooney, D. L. Perry, and L. Illing, eds., pp. 258–267, SPIE, (Bellingham, WA), 1995.
4. B. H. Collins, "Thermal imagery spectral analysis," Master's thesis, Naval Postgraduate School, 1996.
5. S. A. Marino, "Operation and calibration of the nps ulitraviolet imaging spectrometer (nuvis) in the detection of sulfur dioxide plumes," Master's thesis, Naval Postgraduate School, 2000.

*Incidentally, the last eigenvector of the covariance matrix of $\underline{\mathbf{y}}$ was $\hat{\underline{\mathbf{v}}}$, with corresponding eigenvalue $\lambda_N \approx 0$

6. J. S. Tyo, D. I. Dierson, and R. C. Olsen, "Development of an invariant display strategy for spectral imagery," in *Proceedings of SPIE vol. 4132: Imaging Spectrometry VI*, M. R. Descour and S. S. Shen, eds., SPIE, (Bellingham, WA), 2000. In Press.
7. G. Buchsbaum and A. Gottschalk, "Trichromacy, opponent colours coding and optimum colour information transmission in the retina," *Proc. Roy. Soc. Lond. B* **220**, pp. 89–113, 1983.
8. J. Krauskopf, D. R. Williams, and D. W. Heeley, "Cardinal directions of color space," *Vision Res.* **22**, pp. 1123–1131, 1982.
9. K. T. Mullen, "The contrast sensitivity of human colour vision to red-green and blue-yellow chromatic gratings," *J. Physiology (London)* **359**, pp. 381–400, 1985.
10. D. I. Diersen, "Colorimetric representations for hyperspectral imagery," Master's thesis, Naval Postgraduate School, 2000.
11. R. J. Kauth and G. S. Thomas, "The tasselled cap – a graphical description of the spectral-temporal development of agricultural crops as seen by landsat," in *Proceedings of the Symposium on Machine Processing of Remotely Sensed Data*, pp. 4B41–4B51, Purdue University, (West LaFayette, IN), 1976.